Insights from molecular dynamics: What drives the Eu(NO3)3 aggregate formation in solvent extraction?

Lara Žiberna, Philippe Guilbaud, Erwann Guillam, Magali Duvail

Journal of Molecular Liquids 438 (2025) 128711

Contents lists available at ScienceDirect

Journal of Molecular Liquids

journal homepage: www.elsevier.com/locate/molliq

Insights from molecular dynamics: What drives the $Eu(NO_3)_3$ aggregate formation in solvent extraction?

Lara Žiberna [a], Philippe Guilbaud [b], Erwann Guillam [a], Magali Duvail [a,*]

[a] ICSM, Univ Montpellier, CEA, CNRS, ENSCM, Bagnols-sur-Cèze, 30207, France
[b] CEA, DES, ISEC, DMRC, Univ Montpellier, Bagnols-sur-Cèze, 30207, France

HIGHLIGHTS

- We investigated the formation of solvent extraction aggregates composed of $Eu(NO_3)_3$ salts with DMDOHEMA molecules at two salt concentrations using molecular dynamics.
- We pointed out the formation of aggregates mainly consisting of Eu^{3+} monomers and dimers for which the salt concentration only affects the amount of water molecules inside.
- We highlighted that water dynamics and the availability of ligands to form hydrogen bonds are the key points for understanding the aggregation mechanisms.

GRAPHICAL ABSTRACT

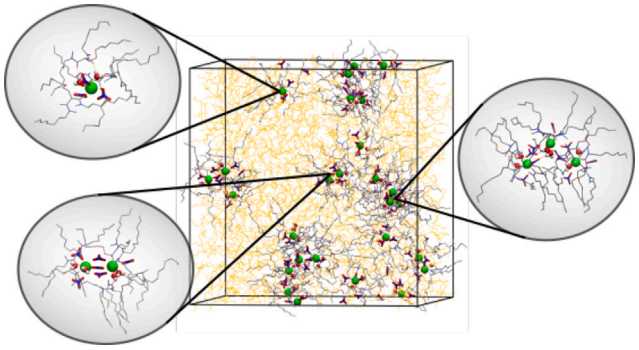

ARTICLE INFO

Keywords:
Lanthanides
Molecular dynamics
Aggregate formation
Solvent extraction phases

ABSTRACT

The study explores the formation of solvent extraction aggregates composed of $Eu(NO_3)_3$ salts with DMDOHEMA molecules solvated in *n*-heptane using classical molecular dynamics simulations at two $Eu(NO_3)_3$ salt concentrations, namely 0.015 and 0.126 mol L^{-1}. For both concentrations, the main aggregates are predominantly in the form of Eu^{3+} monomers and dimers, with a higher ratio of monomers. However, increasing the $Eu(NO_3)_3$ concentration tends to increase the number of dimers. The average Eu^{3+} monomer is composed of three nitrate anions and 3–4 DMDOHEMA molecules, whereas the average dimer is composed of six nitrate anions and 6 DMDOHEMA molecules. For both types of aggregates, the influence of the $Eu(NO_3)_3$ concentration has been observed only in the number of water molecules involved in each kind of aggregate. Furthermore, we demonstrated that the presence of nitrate anions and especially the number of water molecules in the polar core of the aggregates favors the formation of dimers, with various types of nitrate-water bridges. We highlighted that the dynamics of water in the vicinity of the cations, as well as the availability of ligands capable of forming hydrogen bonds within the coordination shell of nearby ions, are crucial for understanding the aggregation mechanisms.

1. Introduction

In the frame of nuclear fuel reprocessing, the recovery of major and minor actinides has been widely studied during the last decades [1–6]. One of the major separation techniques used in this field is the solvent extraction (also known as liquid-liquid extraction) which is based on the relative solubility of different compounds in two non-miscible solvents.

Many processes based on solvent extraction have been developed in this domain like the PUREX (Plutonium Uranium Refining

* Corresponding author.
Email address: magali.duvail@cea.fr (M. Duvail).

https://doi.org/10.1016/j.molliq.2025.128711
Received 23 April 2025; Received in revised form 23 July 2025; Accepted 9 October 2025
Available online 11 October 2025

by EXtraction) process, which is industrially used for more than 50 years [7]. More recently, solvent extraction separation processes have been studied for the separation of americium(III) and curium(III) from the lanthanide(III) cations [8–11]. Among these, the DIAMEX (DIAMide EXtraction) process [12,13] uses the DMDOHEMA (*N*,*N*'-dimethyl-*N*,*N*'-dioctylhexyle-thoxymalonamide) malonamide extractant (Fig. S2, SI), which is also studied outside of the nuclear fuel cycle domain for the separation within the lanthanide cations series [14]. In these separation processes, the malonamide extractants are solvated in an aliphatic diluent. This organic phase is then contacted with an aqueous phase that contains the cation salts to be separated. This aqueous phase is usually an acidic solution resulting from the dissolution, or the leaching of a solid material.

It has been demonstrated that DMDOHEMA extractants can be found in the bulk organic phase or at the interface and that they form aggregates in the presence and absence of ions [15–20]. Indeed, in the absence of ions, DMDOHEMA forms globular aggregates with aggregation numbers between 4 and 10 [15,21–23], whereas in the presence of cation salts, aggregates having a reverse micelles like structures with a well-defined polar core are formed [24–26]. Moreover, the shape and composition of the aggregates also depend on the concentration of co-extracted water in the organic phase [27], which depends on several experimental parameters: i) the concentration of DMDOHEMA, ii) the concentration of nitric acid, and iii) the concentration of the salts extracted in the organic phase [22,28]. For instance, Ellis et al. who studied the formation of lanthanide reverse micelles through the series under acidic and neutral conditions (3 mol L^{-1} HNO_3 or $LiNO_3$ in the aqueous phase, respectively) pointed out that the micelles were larger, more hydrated, and more malonamide extractant molecules participate in the micelles under acidic conditions compared to those formed under neutral conditions [29].

Aggregate formation is of interest because it helps explain differences in extraction coefficients, as fewer diamide molecules per Eu^{3+} ion are required when aggregates are formed [19]. It also sheds light on how the organic phase can separate to form a third phase –a well-known and undesired phenomenon in liquid-liquid extraction processes [30]. Specifically, it has been shown that at high concentrations of nitric acid or cation salts in the organic phase, the attractive force between the aggregates may induce third phase formation, where one phase consists of a low-concentration extractant organic phase, while the other is a high-concentration extractant organic phase containing nitric acid and/or cation salts [18,31]. This is still true in the presence of radioactive cations, as this may lead to criticality problems if there is a high concentration of ions present in one of these two phases [32–34]. Therefore, it is crucial to understand the driving force and mechanism of aggregate formation with malonamide extractants.

In this work, we studied the formation of malonamide aggregates containing $Eu(NO_3)_3$ salts diluted in *n*-heptane using molecular dynamics simulations. Different parameters that influence the aggregation phenomenon have been tested. We first focused on the influence of "experimental" parameters, like the concentrations of $Eu(NO_3)_3$ salt in the organic phase on the aggregate formation. Then, we studied the influence of "theoretical" parameters, typically the influence of the starting aggregate structures on the equilibrium calculated stoichiometries. Here, parameters developed specifically for the lanthanide series with the 12–6-4 Lennard Jones potential have been used [35], and a new method based on the work of Vatin et al. [15] has been employed to analyze the structures of aggregates formed in the organic phase.

2. Methods

2.1. MD simulation details

To explore the $Eu(NO_3)_3$ aggregation behavior in *n*-heptane in the presence of DMDOHEMA molecules at two Eu^{3+} concentrations, we performed molecular dynamics (MD) simulations using PMEMD, a module of the AMBER20 software [36]. Here, the nitrate anions, the *n*-heptane and the DMDOHEMA molecules have been modeled using the force field parameters described in our previous study [35]. The water molecules were described using the 4-site OPC water model [37]. The non-bonded interactions between the Eu^{3+} cations and the molecules present in solution are described by a 12–6-4 Lennard-Jones potential, that takes implicitly into account the polarization thanks to the addition of the $1/r^4$ term [35,38–42]:

$$V_{ij} = \frac{1}{4\pi\varepsilon_0\varepsilon_r}\frac{q_i q_j}{r_{ij}} + \varepsilon_{ij}\left[\left(\frac{R_{\min,ij}}{r_{ij}}\right)^{12} - 2\left(\frac{R_{\min,ij}}{r_{ij}}\right)^{6}\right] - \frac{C_{4,ij}}{r_{ij}^4} \quad (1)$$

where $R_{\min,ij} = 2^{1/6}\times\sigma_{ij}$, and ε_i is linked to $R_{\min,i}/2$ thanks to the noble gas relation [43]

$$\varepsilon_i = 10^{-C_1 \exp\left(-C_2 \times \frac{R_{\min_i}}{2}\right)} \quad (2)$$

with $C_1 = 57.36$ and $C_2 = 2.471$. The crossed C_4 parameters between Eu^{3+} and the other atoms than the water oxygen (C_4(atom type)) were calculated as follows [38]:

$$C_4(\text{atom type}) = \frac{C_4(H_2O)}{\alpha_0(H_2O)} \times \alpha_0(\text{atom type}) \quad (3)$$

where $C_4(H_2O)$ is the C_4 parameter determined for the Eu^{3+} – O_{H_2O} interaction. $\alpha_0(H_2O)$ is the atomic polarizability of the water oxygen (1.444 $Å^3$ [44]) and α_0(atom type) is the atomic polarizability of the atom interacting with the Eu^{3+} cation [45]. For the 12–6 Lennard-Jones parameters, i.e., the non-bonded interactions not involving Eu^{3+}, the classical Berthelot-Lorentz combining rules were used.

An integration step of 1 fs has been used to numerically integrate the equations of motion. Simulations were carried out at 298.15 K in the *NPT* ensemble for the equilibration stage and in the *NVT* ensemble for the production. Periodic boundary conditions were applied. Pressure and temperature were controlled using the Berendsen thermostat and barostat [46]. Long-range interactions were calculated using the particle mesh Ewald summation [47] with a cutoff of 10 Å.

Our investigation focused on two systems with Eu^{3+} concentrations of 0.015 and 0.126 mol L^{-1}, both systems containing 0.5 mol L^{-1} of DMDOHEMA extractant. The concentration of water co-extracted into the organic phase for both systems was taken from the experimental work of Ellis et al. [19], i.e., a concentration of 0.070 and 0.246 mol L^{-1} for the 0.015 and 0.126 mol L^{-1} of Eu^{3+}, respectively.

To establish a reliable starting point, we initially modeled a box with 334 *n*-heptane molecules, one $Eu(NO_3)_3$ salt, and the numbers of water, DMDOHEMA and *n*-heptane molecules corresponding to the experimental concentrations. That is, 5 water molecules and 34 DMDOHEMA molecules solvated in 334 *n*-heptane molecules for the Eu^{3+} concentration of 0.015 mol L^{-1}, and 2 water molecules and 4 DMDOHEMA molecules solvated in 40 *n*-heptane molecules for the Eu^{3+} concentration of 0.126 mol L^{-1}. The boxes were generated with PACKMOL [48] and equilibrated in the *NPT* ensemble during 1 ns using the SANDER module of AMBER20 [36]. For both concentrations, we obtained an aggregate composed of one Eu^{3+} cation, three NO_3^- anions, two DMDOHEMA molecules, and two water molecules in the Eu^{3+} first coordination shell (Fig. 1(a) and (b)). For simplicity, we will refer to these two systems as **LowC**1 and **HighC**1 for the Eu^{3+} concentration of 0.015 and 0.126 mol L^{-1}, respectively.

Moreover, this equilibration process was repeated to establish alternative starting configurations referred to as **LowC**2 and **HighC**2 at low and high Eu^{3+} concentrations, respectively. For the **LowC**2 system, the aggregate obtained consisted of two NO_3^- anions, three DMDOHEMA molecules, and two water molecules in the Eu^{3+} first coordination shell (Fig. 1(c)), whereas for the **HighC**2 system, it comprised three NO_3^- anions, two DMDOHEMA molecules, and one water molecule in the Eu^{3+}

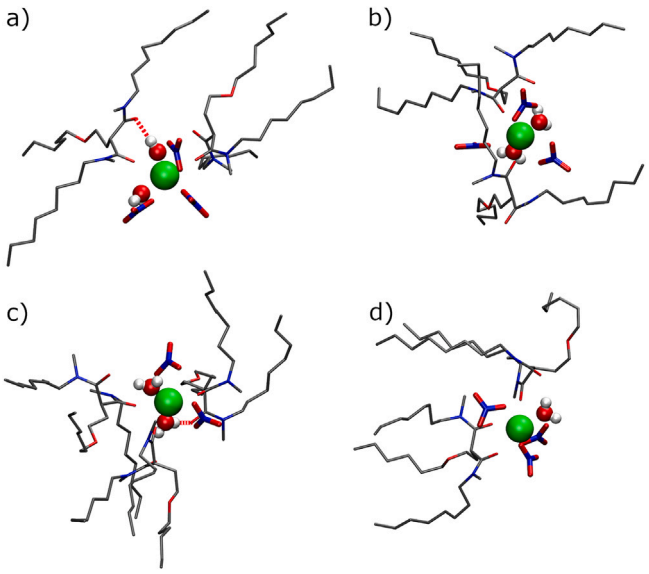

Fig. 1. Snapshots issued from MD simulations showing the starting points used for the (a) **LowC**1, (b) **HighC**1, (c) **LowC**2, and (d) **HighC**2 systems. The Eu^{3+} cations are represented in green, the oxygen atoms in red, the nitrogen atoms in blue, the carbon atoms in dark gray, and the hydrogen atoms in white. For clarity, the hydrogen atoms of the DMDOHEMA carbon chains are not represented.

Table 1
Numbers of molecules in the MD simulation boxes.

	C = 0.015 mol L^{-1}	C = 0.126 mol L^{-1}
	LowC1 & **LowC**2	**HighC**1 & **HighC**2
Eu^{3+}	27	27
NO_3^-	81	81
DMDOHEMA	918	108
H_2O	135	54
n-heptane	9018	1080

first coordination shell (Fig. 1(d)). Note that, for the **LowC**2 system, the third nitrate anion is located in the Eu^{3+} third coordination sphere.

In summary, at the end of the equilibration process, four distinct systems were generated. Two with the same starting aggregate stoichiometry, but at different Eu^{3+} concentrations (0.015 mol L^{-1} and 0.126 mol L^{-1}), referred to as **LowC**1 and **HighC**1, and two with different starting aggregate stoichiometries for each concentration, referred to as **LowC**2 and **HighC**2. Subsequently, the four simulation boxes were replicated 27 times to generate larger simulation boxes. The numbers of molecules present in each system are detailed in Table 1. After a 500 ps equilibration stage in the NPT ensemble, performed on the larger simulation boxes to ensure constant density, all systems were simulated in the NVT ensemble for 100 ns, and analyses were performed on the final 50 ns of the simulations.

2.2. Aggregate analysis

To investigate the Eu^{3+} aggregates, we analyzed the internal distances within the aggregate by computing radial distribution functions (RDFs) between Eu^{3+} and the coordinating atoms of the solvated ligands using the VMD software [49]. To study in detail the composition and formation of the aggregates in our system, we used the MDAnalysis Python package [50,51]. Based on distance criteria deduced from the RDFs, we determined which molecules are located in the aggregate. To this end, we first determined the interactions between the Eu^{3+} cation and the coordinating oxygen atoms of the ligand within its primary coordination shell by using the distance at the base after the first RDF peak. Subsequently, a second set of connection distances was used, focusing on the hydrogen bond formation between the molecules in the Eu^{3+} first sphere and those in its second sphere. To determine the formation of Eu^{3+} oligomers, such as dimers and trimers, we calculated the overlap of the second spheres of the Eu^{3+} monomers. This last step is crucial for accurately determining the number of molecules within each oligomer. A detailed explanation of the code developed here can be found in the Supporting Information. Note that, in this paper, the phrases monomer, dimer, trimer, etc. refer to the total number of Eu^{3+} cations in the aggregate.

3. Results and discussion

3.1. Influence of the concentration

First, we investigate the influence of the concentration of europium salts on the structural properties of aggregates in the system. To achieve this, we conducted simulations on two systems where we used identical Eu^{3+} complex compositions as a starting point: an aggregate consisting of one Eu^{3+} ion, three NO_3^- anions, two H_2O molecules, and two DMDOHEMA molecules solvated in a mixture composed of *n*-heptane, H_2O and DMDOHEMA molecules to reach the corresponding concentrations of systems **LowC**1 and **HighC**1. These aggregates correspond to snapshots given in Fig. 1(a) and (b).

To determine the ligand coordination around the Eu^{3+} ion for systems **LowC**1 and **HighC**1, we calculated the RDFs between the Eu^{3+} cations and NO_3^- anions, DMDOHEMA and H_2O molecules (Figs. S3 and S4, SI). Both the DMDOHEMA molecules and the NO_3^- anions may adopt two coordination modes in the Eu^{3+} first coordination shell: monodentate or bidentate. These two coordination modes are observed in the Eu^{3+} – $C_{DMDOHEMA}$ (Figs. S3(a) and S4(a), SI) and Eu^{3+} – $N_{NO_3^-}$ (Figs. S3(b) and S4(b), SI) RDFs. For each RDF, we observed two well-defined peaks corresponding to the Eu^{3+} first coordination shell, i.e., between 3.8 and 5.4, and between 2.8 and 4.2 Å for DMDOHEMA and NO_3^-, respectively. The bidentate binding mode results in shorter distances between the Eu^{3+} and $C_{DMDOHEMA}$ or $N_{NO_3^-}$, compared to the monodentate ones. By integrating the RDFs, we calculated the number of corresponding atoms around Eu^{3+} for each RDF peak. All distances and the corresponding numbers of atoms are presented in Table 2. We found that the total coordination number of Eu^{3+}, calculated as the total number of oxygen atoms in the Eu^{3+} first coordination shell, is 8.9 for **LowC**1 and 9 for **HighC**1.

Table 2
Distances between Eu^{3+} and the relevant atoms of the molecules forming the micelles (d), and corresponding numbers of atoms (N) calculated from MD simulations at different concentrations and with the different starting points.

	C = 0.015 mol L^{-1}				C = 0.126 M			
	LowC1		**HighC**1		**LowC**2		**HighC**2	
Path	d^a	N	d^a	N	d^a	N	d^a	N
DMDOHEMA								
Eu^{3+} – $O_{DMDOHEMA}$	2.44	2.7	2.41	3.2	2.44	2.1	2.41	3.5
Eu^{3+} – $C^{bi}_{DMDOHEMA}$	4.10	0.5	4.10	0.6	4.11	0.2	4.10	1.2
Eu^{3+} – $C^{mono}_{DMDOHEMA}$	4.70	1.7	4.60	1.9	4.68	1.7	4.65	1.1
Nitrate								
Eu^{3+} – $O_{NO_3^-}$	2.39	3.0	2.39	3.8	2.39	3.1	2.39	3.7
Eu^{3+} – $N^{bi}_{NO_3^-}$	2.97	0.1	2.93	0.6	2.97	0.1	2.94	0.2
Eu^{3+} – $N^{mono}_{NO_3^-}$	3.60	2.9	3.54	2.6	3.58	2.9	3.58	3.2
Water								
Eu^{3+} – O_{H_2O}	2.39	3.2	2.38	2.0	2.39	3.7	2.38	1.8
Total coordination number		8.9		9.0		8.9		9.0

[a] in Å.

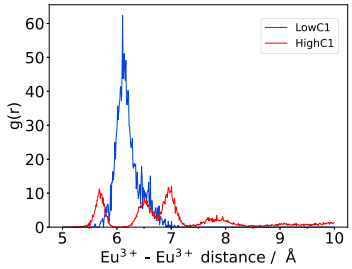

Fig. 2. Eu^{3+} – Eu^{3+} RDF calculated for the **LowC**1 (blue) and **HighC**1 (red) simulations.

Our findings indicate that the concentration of Eu^{3+} cations has only a minor influence on the binding mode of DMDOHEMA molecules and NO_3^- anions. Specifically, a higher number of bidentate and monodentate DMDOHEMA molecules is observed at high concentration (**HighC**1), while monodentate coordination of NO_3^- anions is greater at low concentration (**LowC**1). However, the trend remains the same: DMDOHEMA molecules and NO_3^- anions preferentially bind in a monodentate mode rather than in a bidentate mode. Furthermore, concentration has almost no effect on the distances between the Eu^{3+} cation and the coordinating ligands, nor on the coordination number of Eu^{3+}. The difference in coordination number between **LowC**1 and **HighC**1 might originate from a higher number of DMDOHEMA molecules and NO_3^- anions coordinating in the bidentate mode at **HighC**1 compared to **LowC**1. The calculated distances and coordination numbers show good agreement with previous studies that have investigated Eu^{3+} aggregation in the bulk organic phase across various concentrations [19,29,52]. This consistency not only validates the reliability of our model, but also reinforces confidence in its ability to describe the fundamental interactions governing aggregation behavior. Further, by extending the simulation times, we ensure that the system reaches better equilibration. This enables a more thorough investigation of the aggregate composition and its evolution over longer timescales, providing deeper insights into the structural organization of the aggregates.

In both simulations (**LowC**1 and **HighC**1), we observed that aggregates coalesce to form oligomers in the bulk organic phase, driven by the strong electrostatic interactions between the species. This requires further investigation into the mechanism underlying the formation of such oligomers and the impact of the Eu^{3+} concentration on the number of oligomers formed. To investigate the mechanism of oligomer formation, the RDFs between the Eu^{3+} cations were calculated for both **LowC**1 and **HighC**1 (Fig. 2). We observed several peaks, each representing a stable mode of Eu^{3+} — Eu^{3+} connection. In such aggregates or oligomers, various connection types between the Eu^{3+} exist, as they mainly depend on the Eu^{3+} — Eu^{3+} distance and the position of the ligands around them. The main connection types are represented in Fig. 3. The connections are shown as a function of the distance between Eu^{3+} cations. We noticed that the main connection types are made of NO_3^- and NO_3^- – H_2O bridges, where the NO_3^- anion forms a hydrogen bond with the H_2O molecule. At the shortest distance, typically 5.5 Å - 6.0 Å, the bridge is formed with three nitrate ions (Fig. 3(a)). On the contrary, at the largest distance, typically 9.7 Å, the two cations are connected by a single NO_3^-–H_2O bridge (Fig. 3(f)). Between these two distances, we observed the formation of NO_3^- bridges, NO_3^-–H_2O bridges or the combination of the two.

The connections between two Eu^{3+} ions are facilitated by the molecules surrounding the ion (NO_3^- anions and H_2O molecules), which bind to another Eu^{3+} ion or form hydrogen bonds with each other, serving as the main driving force for the formation of aggregates. The type of connection predominantly depends on the availability of such molecules and their ability to form hydrogen bonds. These connection modes are observed at both concentrations, indicating that concentration does not significantly influence the binding mechanism. However,

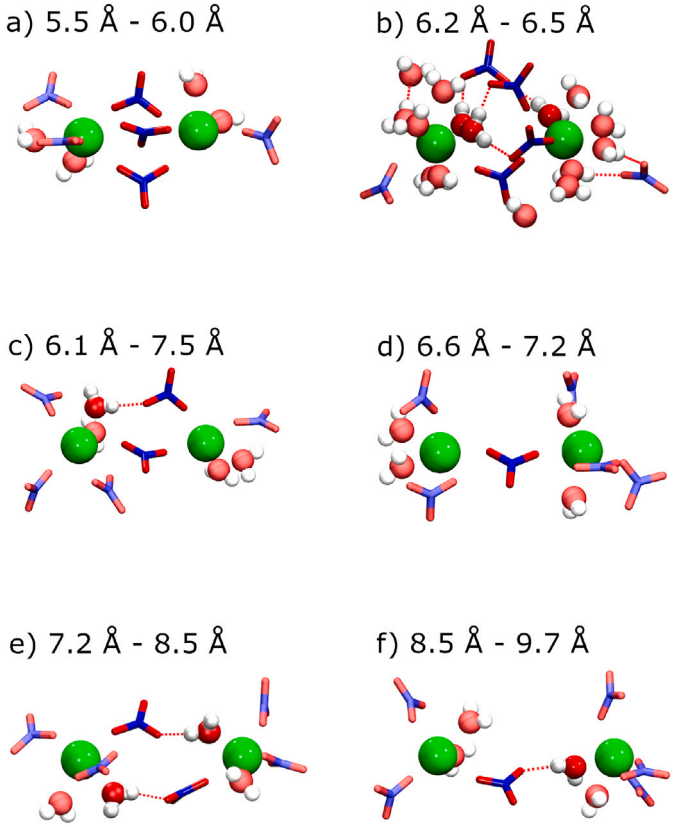

Fig. 3. Snapshots issued from MD simulations showing the various types of connection between two Eu^{3+} cations for a Eu^{3+} – Eu^{3+} distance of (a) 5.5 - 6,0 Å, (b) 6.2 – 6.5 Å, (c) 6.1 – 7.5 Å, (d) 6.6 – 7.2 Å, (e) 7.2 – 8.5 Å, and (f) 8.5 – 9.7 Å. The same colors as in Fig. 1 have been used.

we observed that in the **LowC**1 system, the Eu^{3+} – Eu^{3+} connection is primarily formed by NO_3^- – H_2O, in contrast to the **HighC**1 system, where all types of connections are present. This difference may stem from the varying hydration states of the aggregates, as the total number of water molecules per Eu^{3+} cation is higher at **LowC**1 than at **HighC**1 (Table 1). The spatial arrangement of the NO_3^- anions and H_2O molecules, and the distance between the Eu^{3+} cations thus play a crucial role in determining the nature of the interactions. This is further confirmed experimentally and theoretically by Qiao et al. [53] who studied aggregate size and shape and demonstrated that NO_3^- bridges were detected at shorter distances, while NO_3^-–H_2O and DMDOHEMA–NO_3^- bridges were observed at longer distances. Here, we observed NO_3^- bridges at shorter distances, along with NO_3^-–H_2O and the combination of NO_3^--H_2O bridges. However, the bridging patterns differ significantly. Indeed, in the work of Qiao et al., they reported four or two NO_3^- anions forming a bridge; here we observed configurations with either three or one NO_3^- anion. These findings support our hypothesis that Eu^{3+}–Eu^{3+} bridges form randomly, depending on the availability of nearby ligands capable of establishing hydrogen bonds within the coordination shell of nearby ions.

Furthermore, we investigated how the concentration impacts the number of oligomers formed during the simulation and their compositions. The first coordination shell around the central Eu^{3+} ion consists of NO_3^- anions, H_2O and DMDOHEMA molecules, that are coordinating the Eu^{3+} cation with oxygen atoms. The molecules present in the second coordination shell form hydrogen bonds with the molecules in the first shell. To obtain information about the average composition of the aggregates we calculated previously, the RDFs between the Eu^{3+} ion and the central carbon atom of the DMDOHEMA molecule, the nitrogen

Table 3
Distance cutoffs (in Å) used to calculate the number of ligands in the aggregates.

Path	Cutoff distance[a]
First coordination shell	
$Eu^{3+} - O_{DMDOHEMA}$	3.60
$Eu^{3+} - O_{NO_3^-}$	3.20
$Eu^{3+} - O_{H_2O}$	3.20
Second coordination shell	
$O_{DMDOHEMA} - H_{H_2O}$	2.40
$O_{NO_3^-} - H_{H_2O}$	2.35
$O_{H_2O} - H_{H_2O}$	2.40

[a] in Å.

atom of NO_3^- anions, and the oxygen atom of the H_2O molecules. In this way, we obtained the average number of DMDOHEMA molecules, NO_3^- anions and H_2O molecules around the Eu^{3+} ion. However, this does not allow us to study the aggregate composition in detail. This is especially true for aggregates containing more than one Eu^{3+} ion, where the binding modes are more complex than in aggregates containing a single one Eu^{3+} ion. Therefore, to study the internal bonding in the aggregates, we developed a code based on cutoff distances between the Eu^{3+} ion and the coordinating oxygen atoms of NO_3^- anions, DMDOHEMA, and H_2O molecules, as well as the distances between the species in the first and second sphere that can form hydrogen bonds. This allows us to study each aggregate separately and determine the differences between the monomers, comprising only one Eu^{3+} ion, and larger aggregates with more than one Eu^{3+} ion. The detailed functionality of the code is available in the Supporting Information. The cutoff distances were calculated from the RDFs between Eu^{3+} and the atoms directly bonded to it: the ketone oxygen atoms of DMDOHEMA, namely $O_{DMDOHEMA}$ (Figs. S3(c) and S4(c), SI), and the oxygen atoms of NO_3^-, namely $O_{NO_3^-}$ (Figs. S3(d) and S4(d), SI) and H_2O, namely O_{H_2O} (Figs. S3(e) and S4(e), SI), by considering the distance that corresponds to the end of the first coordination shell position. To determine the second coordination shell, the RDFs between the hydrogen atoms of the H_2O molecules (H_{H_2O}) in the Eu^{3+} first coordination shell and the oxygen atoms of the DMDOHEMA molecules (Figs. S5(a) and S6(a), SI), NO_3^- (Figs. S5(b) and S6(b), SI) and H_2O (Figs. S5(c) and S6(c), SI) in the Eu^{3+} second coordination shell were used. All the cutoff distances are given in Table 3.

For the **LowC**1 simulation, we obtained on average 25 monomers and 1 dimer, as seen in Fig. 4 in blue. A detailed analysis of the time-averaged composition of Eu^{3+} aggregates reveals that the Eu^{3+} monomers are composed of 3 NO_3^- anions, 2 to 8 H_2O molecules, and 2 to 7 DMDOHEMA molecules (Fig. 5(a)). The average stoichiometry calculated for the Eu^{3+} monomers is 3.0 nitrate anions, 4.5 water molecules, and 4.4 DMDOHEMA molecules, whereas for the Eu^{3+} dimer it is 6.0 nitrate anions, 17.6 water molecules, and 6.3 DMDOHEMA molecules (Table S1, SI). Note that some water molecules (less than five) do not participate in Eu^{3+} oligomers, they are present in the bulk in

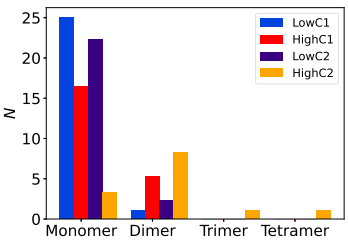

Fig. 4. Average numbers of Eu^{3+} monomers, dimers, trimers and tetramers formed during the simulations **LowC**1 (blue), **HighC**1 (red), **LowC**2 (purple), and **HighC**2 (orange).

interaction with DMDOHEMA molecules, as already observed by Vatin et al. [15]. Here, we observed that some monomers exhibited a relatively high number of water molecules, typically 6–8 (Fig. 5), which exceeds the number of water molecules per Eu^{3+} cation in the simulation box, namely 5. Note that these numbers correspond to total numbers of water molecules in both the Eu^{3+} first and second coordination shells. By analyzing in more detail the time-averaged compositions of the Eu^{3+} first coordination shell, we observed that configurations with up to 7 water molecules in the Eu^{3+} first coordination shell are calculated (Fig. S7(a), SI). However, the occurrence of these highly hydrated monomers is low, and to compensate, there are some monomers with very few water molecules present. For monomers with a high number of water molecules in the Eu^{3+} first coordination shell, NO_3^- anions and DMDOHEMA molecules remain mainly in the Eu^{3+} second coordination as the fully hydrated stoichiometry is 9 [35] (Fig. S8(a), SI). Therefore, the presence of NO_3^- anions and DMDOHEMA molecules in the second coordination shell of Eu^{3+} monomers increases the likelihood of monomers forming a dimer due to the numerous opportunities for hydrogen bonds among the ligands and the availability of NO_3^- anions to form bridging interactions. As a result, the dimer is characterized by an increased water content (17.6 on average). Indeed, although the number of water molecules in the Eu^{3+} dimer is much larger than that of the Eu^{3+} monomer, the ratio between both stoichiometries is 3.9, which is comparable to that calculated by Ellis et al. (3.8). Regarding the DMDOHEMA molecules, their number in the Eu^{3+} dimer is noticeably less than twice that in the monomer, which is in agreement with the findings of Ellis et al. (i.e., $Eu(NO_3)_3(H_2O)_{0.8}(DMDOHEMA)_3$ and $Eu_2(NO_3)_6(H_2O)_3(DMDOHEMA)_4$), who related this with the increase of the distribution ratio when the concentration of Eu^{3+} increases initially in the aqueous phase: the more Eu^{3+} cations are extracted, the less DMDOHEMA extractants are needed for their extraction [19]. Detailed analysis of the time-averaged composition of the aggregates shows that the maximum number of DMDOHEMA molecules in the Eu^{3+} first coordination shell is for the monomer, while almost all DMDOHEMA molecules in the dimers are in its second coordination shell (Fig. S8(a), SI). In addition, not all of the DMDOHEMA molecules are bonded in the Eu^{3+} aggregates. Indeed, a total of 802 “free” DMDOHEMA molecules, corresponding to a concentration of 0.41 mol L^{-1}, are found in the bulk organic phase for **LowC**1.

For the **HighC**1 simulation, we obtained an average of 16.5 monomers and 5.3 dimers of Eu^{3+} (Fig. 4 in red). The time-averaged composition analysis of the Eu^{3+} aggregates indicates that the average Eu^{3+} monomer consists of 3.0 NO_3^- anions, 2.0 H_2O molecules, and 3.6 DMDOHEMA molecules, and the Eu^{3+} dimer on average contains 6.0 NO_3^- anions, 4.0 H_2O molecules, and 6.2 DMDOHEMA molecules (Fig. 5(b)). As already observed for the **LowC**1 system, the maximum number of DMDOHEMA participating to the Eu^{3+} monomer in the Eu^{3+} first coordination shell is three. However, contrary to what was observed for the dimers formed at **LowC**1, up to five DMDOHEMA molecules may be present within the first and the second cation coordination spheres (Fig. S8(b), SI). This might originate from the low water content in the dimer, typically four water molecules in the Eu^{3+} first coordination shells (Fig. S7(b), SI), which corresponds to the number of H_2O molecules present in the simulation box per Eu^{3+} cation (which is 2). Furthermore, as already mentioned, the average number of DMDOHEMA per Eu^{3+} cation in dimers is not twice that in monomers, and, 18 free DMDOHEMA molecules remain in the bulk organic phase, which corresponds to a much lower concentration of free DMDOHEMA extractants (0.08 mol L^{-1}) compared to what was obtained for **LowC**1. Finally, almost no free H_2O molecules (0.002 molecules) are present in the organic phase. Under these conditions, the organic phase is close to saturation in $Eu(NO_3)_3$ salt.

In the literature, the aggregation of Eu^{3+} ions in the organic phase with DMDOHEMA extractant was studied experimentally and theoretically. Muller et al. investigated the aggregation of Eu^{3+} ions in organic phase containing DMDOHEMA extractant

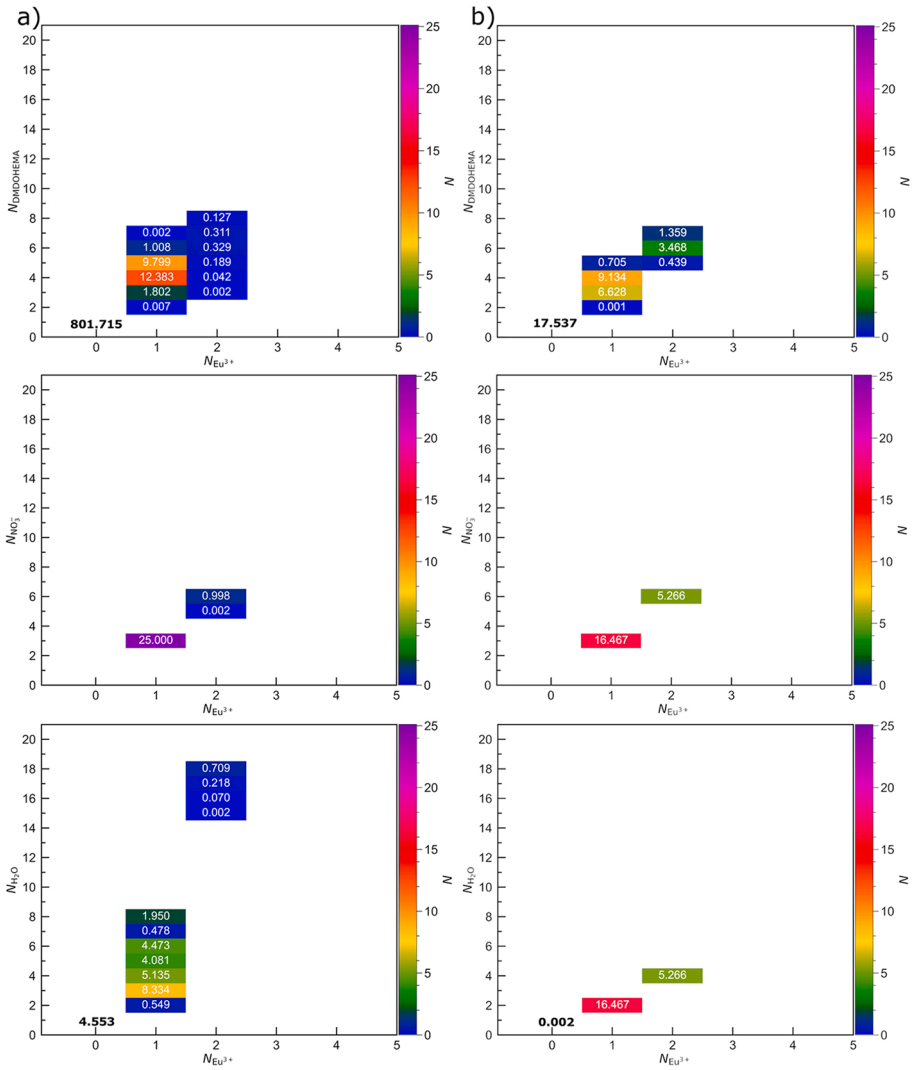

Fig. 5. Composition maps of Eu^{3+} aggregates for (a) **LowC**1 and (b) **HighC**1. Color levels indicate the time-averaged numbers of Eu^{3+} aggregates, N, also shown in white on each tile. Values at position 0 represent free molecules not participating in Eu^{3+} aggregates.

by spectroscopic techniques and DFT calculations, and they have found that Eu^{3+} aggregates were formed with a stoichiometry of $Eu(NO_3)_3(H_2O)_{1-2}(DMDOHEMA)_{2-4}$ [54]. Similarly in the experimental and theoretical study of Meridiano et al., they found that when the aqueous phase, containing $Eu(NO_3)_3$ and $LiNO_3$ salts, is contacted with an organic phase containing 0.5 mol L^{-1} of DMDOHEMA, Eu^{3+} cations form aggregates with a stoichiometry of $Eu(NO_3)_3(DMDOHEMA)_4$ [55]. Moreover, Ellis et al. who investigated the Eu^{3+} aggregation in organic phase found that for the Eu^{3+} concentrations of 0.015 mol L^{-1} the aggregates formed have average stoichiometries of $Eu(NO_3)_3(H_2O)_{0.8}(DMDOHEMA)_3$ and $Eu_2(NO_3)_6(H_2O)_3(DMDOHEMA)_4$) for the Eu^{3+} monomer and dimer, respectively [19]. In our study, we calculated monomer aggregates with a stoichiometry in line with the literature, but further we observed the significant influence of the Eu^{3+} concentration on the number of aggregates formed. Indeed, the higher the Eu^{3+} concentration, the larger the number of aggregates formed. The average aggregate composition analysis reveals that the number of DMDOHEMA molecules per Eu^{3+} cation increases non-linearly when comparing the monomers and dimers for both concentrations. However, the average numbers of DMDOHEMA molecules and NO_3^- anions per monomer or dimer remain consistent at both concentrations. In contrast, the number of water molecules differs significantly, with a substantially higher presence of water within the aggregates in the **LowC**1 simulation.

3.2. *Influence of the starting point*

Here, we investigate the influence of the starting point on the formation and composition of the aggregates. This was achieved by maintaining identical Eu^{3+} concentrations as previously, i.e., 0.015 and 0.126 mol L^{-1}, while varying the initial configuration of the aggregates (Fig. 1). In the simulation where the Eu^{3+} concentration is 0.015 mol L^{-1} (**LowC**2), the initial aggregate is composed of two NO_3^- anions, three DMDOHEMA and two H_2O molecules in the Eu^{3+} first coordination shell, whereas for the **HighC**2 simulation, it is composed of three NO_3^- anions, two DMDOHEMA molecules, and one H_2O molecule in the Eu^{3+} first coordination shell (Fig. 1(c) and (d)). To understand the effect of the starting point on the aggregate compositions, we compare **LowC**1 with **LowC**2, and **HighC**1 with **HighC**2.

Similarly to the previous analyses, we determined the cutoff distances by analyzing the RDFs between the central Eu^{3+} cation and the coordinating ligands (Figs. S9 and S10, SI) and between the ligands present in the Eu^{3+} first and second coordination shells (Figs. S11 and S12, SI). The distances are reported in Table 2. Our results do

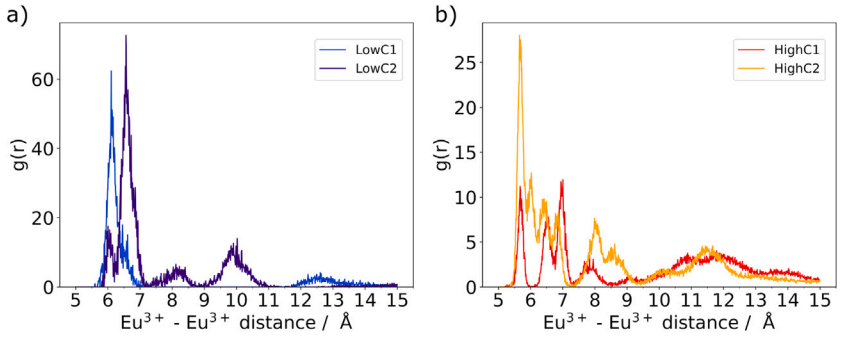

Fig. 6. Eu^{3+}–Eu^{3+} RDF calculated for Eu^{3+} concentrations of (a) 0.015 mol L^{-1}: **LowC**1 (blue) and **LowC**2 (purple), and (b) 0.126 mol L^{-1}: **HighC**1 (red) and **HighC**2 (orange).

not indicate significant differences in terms of distance between the Eu^{3+} cation and the coordinating ligands when comparing simulations at low and high concentrations. When comparing **LowC**1 and **LowC**2, the coordination numbers show minor variations, yet both demonstrated the same trend: for both concentrations simulations, more DMDOHEMA molecules and NO_3^- anions are bonded in the monodentate mode than in the bidentate mode. However, when we compare **HighC**1 and **HighC**2 we observe that, for the **HighC**2 simulation, more DMDOHEMA molecules are bonded in the bidentate mode than in the monodentate mode, which contrasts with the behavior observed in simulation **HighC**1. This might be the consequence of the difference in the binding mode of DMDOHEMA in the initial aggregate, where, for the **HighC**1 system, both DMDOHEMA molecules are bonded in monodentate mode, but for the **HighC**2 system, one of the two DMDOHEMA molecules present in the initial aggregate is bonded in bidentate mode. The NO_3^- anions predominantly bonded the Eu^{3+} cation in the monodentate mode regardless of the starting point, as already observed. It originates from the presence of water molecules in the Eu^{3+} first coordination (1.8–3.7) [56]. To study the coordination number, we calculated the RDFs between Eu^{3+} and the coordinating atoms (oxygen atoms of DMDOHEMA, H_2O and NO_3^-). By integrating the peaks we calculated total coordination numbers of 8.9 and 9 for **LowC**2 and **HighC**2, respectively, as already calculated for **LowC**1 and **HighC**1.

Further, we examined the influence of the starting point on the formation of Eu^{3+} oligomers, first looking at the Eu^{3+}–Eu^{3+} RDFs (Fig. 6). The Eu^{3+}–Eu^{3+} RDF calculated for **LowC**2 and **HighC**2 simulations exhibits additional peaks compared to **LowC**1 and **HighC**1, respectively (Fig. 6). In fact, the Eu^{3+} dimers experience a greater variety of connections in the **LowC**2 and **HighC**2 simulations. However, in all cases, the connection types remain the same: NO_3^- bridges, NO_3^-–H_2O bridges and the combinations of the two. Furthermore, as already mentioned, the NO_3^- bridges connection types between the Eu^{3+} cations is predominant at short Eu^{3+}–Eu^{3+} distances, while combinations of NO_3^- and NO_3^- – H_2O bridges are observed for intermediate Eu^{3+}–Eu^{3+} distances, and NO_3^- – H_2O bridges at large Eu^{3+}–Eu^{3+} distances. In addition, for the **HighC**2 simulation, we observed another connection type never found before, neither at low concentration nor in the **HighC**1 simulation, where a DMDOHEMA molecule forms H-bonds with water molecules forming a bridge between two Eu^{3+} cations, as shown in Fig. 7. A similar connection was observed in the work of Qiao et al., where they found DMDOHEMA bridging through NO_3^-, while we only observed DMDOHEMA forming a bridge via water molecules only. This connection corresponds to the Eu^{3+}–Eu^{3+} distance of the last peak, i.e., 11.5 Å (Fig. 6(b)).

As mentioned above, the connections between two Eu^{3+} cations are primarily facilitated by hydrogen bonds formed between the ligands. As a result, the spatial arrangement of these ligands plays a crucial role in the formation of such connections. Here, we observed that different starting points affect these connections, mainly due to variations in the positioning of the ligands around the Eu^{3+} cation.

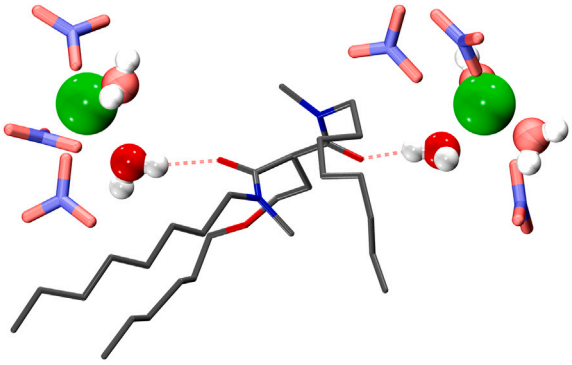

Fig. 7. Snapshot issued from the **HighC**2 MD simulation showing a DMDOHEMA molecule forming a bridge between two Eu^{3+} cations with two H_2O molecules belonging each to the Eu^{3+} first coordination shells.

The observed differences in connections further confirm that the formation of these connections is indeed dependent on the arrangement of the ligands. However, it should be noted that the connection involving a DMDOHEMA ligand between two Eu^{3+} cations is very rare, as it occurred in only one Eu^{3+} dimer yet persisted throughout the entire **HighC**2 simulation.

As already performed for the **LowC**1 and **HighC**1 systems, we compared the time-averaged compositions of the Eu^{3+} aggregates formed (Fig. 8). In the **LowC**2 simulation the system is composed on average of 22.4 Eu^{3+} monomers and 2.3 Eu^{3+} dimers (Fig. 4). Although there is a difference in the number of Eu^{3+} monomers and dimers formed compared to **LowC**1, where 25 monomers and 1 dimer are present, this difference is relatively small and does not indicate a significant deviation in the overall species distribution. However, this slight difference in the number of oligomers formed may result from different spatial orientations of the ligands around the Eu^{3+} ion. Indeed, this is mostly because, at the starting point of **LowC**2, only two NO_3^- anions are present in the Eu^{3+} first coordination sphere. During the simulation, the third NO_3^- anion, initially outside the Eu^{3+} first sphere, enters it, causing the spatial rearrangement of the ligands that can promote dimer formation.

For the **LowC**2 simulation, the numbers of DMDOHEMA molecules per Eu^{3+} cation are consistent with those calculated for the **LowC**1 simulation. However, the number of NO_3^- anions in the Eu^{3+} monomers fluctuates between 2 and 3. This is directly related to the initial starting point configuration of this simulation, where 2 NO_3^- anions are in the first coordination sphere and the third is outside. Since the NO_3^- anions do not all enter the aggregate simultaneously, fluctuations arise between monomers containing only two NO_3^- anions and those with three. Nevertheless, the number of monomers with only two NO_3^- anions remains low and continues to decrease as the simulation progresses,

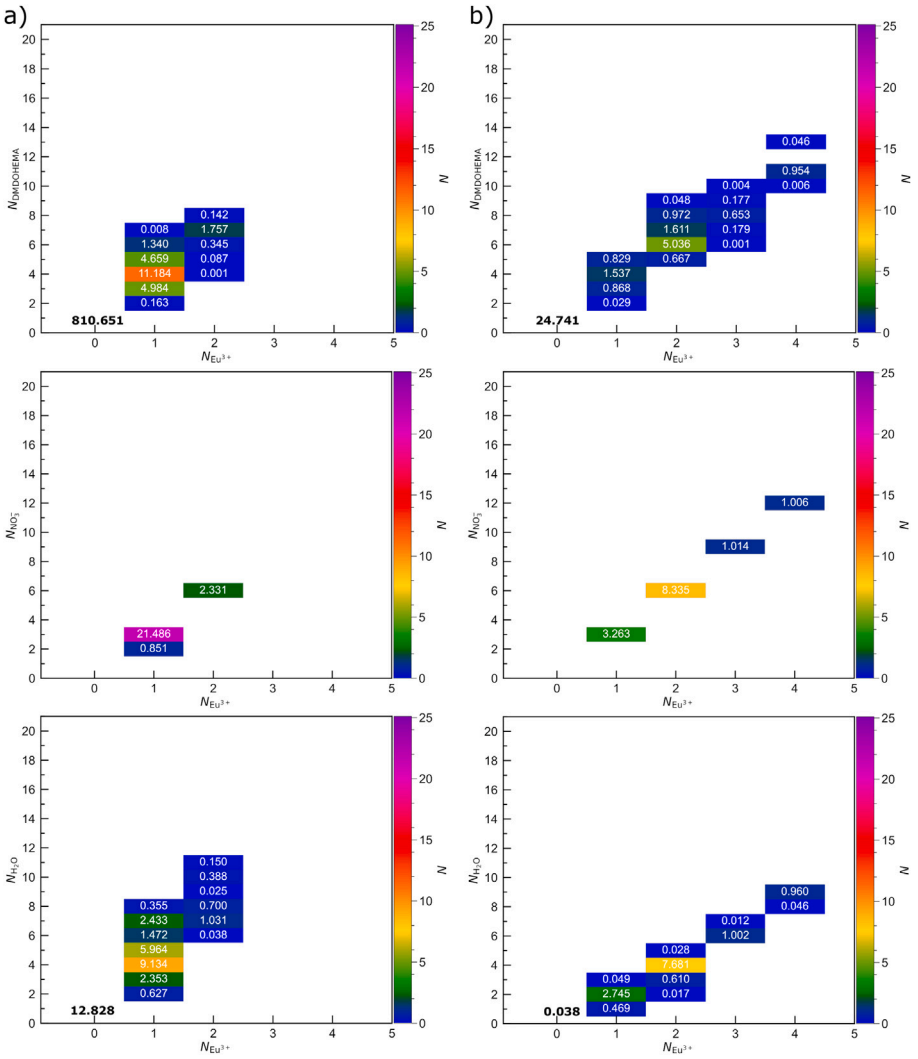

Fig. 8. Composition maps of Eu^{3+} aggregates for (a) **LowC**2 and (b) **HighC**2. Color levels indicate the time-averaged numbers of Eu^{3+} aggregates, N, also shown in white on each tile. Values at position 0 represent free molecules not participating in Eu^{3+} aggregates.

with additional NO_3^- anions incorporating into the aggregate. As a result, the final average stoichiometry of Eu^{3+} monomers consists of 3.0 NO_3^- anions, 4.6 water molecules, and 4.1 DMDOHEMA molecules, which is similar to the one calculated for the **LowC**1 system (Table S1, SI). Indeed, quite a large number of water molecules are calculated in the Eu^{3+} first coordination shell (up to 6), promoting the formation of highly hydrated Eu^{3+} dimers (Fig. S7(c), SI). The average Eu^{3+} dimer contains 6.0 NO_3^- anions, 8.1 water molecules, and 6.8 DMDOHEMA molecules. In the bulk organic phase, free DMDOHEMA molecules remain corresponding to a concentration of 0.41 mol L^{-1} which is similar to the **LowC**1 simulation. Indeed, the stoichiometries of DMDOHEMA molecules involved in the Eu^{3+} monomers and dimers are nearly identical between **LowC**1 and **LowC**2 (Table S1, SI) implying that almost the same number of DMDOHEMA participate in the oligomer formation. The only difference lies in the number of water molecules involved in the oligomers. Indeed, for the **LowC**1 simulation, only one dimer is present, in which more water molecules participate compared to the **LowC**2 simulation. Here, a large number of water molecules, typically 6.2 on average, are present in the second shell of the aggregate (Table S1, SI).

For the **HighC**2 simulation, we calculated on average 3.3 monomers, 8.3 dimers, one trimer, and one tetramer (Fig. 4). The analysis of the time-averaged composition of the aggregates allows us to determine that the average Eu^{3+} monomer is composed of 3.0 NO_3^- anions, 1.9 H_2O molecules, and 4.0 DMDOHEMA molecules. This is followed by the dimer $Eu_2(NO_3)_6(H_2O)_{3.9}(DMDOHEMA)_{6.4}$, the trimer $Eu_3(NO_3)_9(H_2O)_6(DMDOHEMA)_8$, and the tetramer $Eu_4(NO_3)_{12}(H_2O)_9(DMDOHEMA)_{11.1}$ (Fig. 8(b)). Compared to the average Eu^{3+} monomer stoichiometry calculated for **HighC**1, i.e., $Eu(NO_3)_3(H_2O)_2(DMDOHEMA)_{3.6}$ (Table S1, SI), we observed that the starting point does not significantly influence the composition of the monomer. Although the **HighC**2 initial configuration contains only one H_2O molecule in the Eu^{3+} first coordination shell, compared to two in the **HighC**1 initial configuration, we observed a higher fluctuation in the number of water molecules for the **HighC**2 system (Figs. 5(b) and 8(b), and Fig. S7(b)–(d), SI). Indeed, it appears that the maximum ratio between cations and water, namely 1:2, is already reached at the beginning of the **HighC**1 simulation, whereas the equilibrium process occurs during the **HighC**2 simulation. Finally, the concentration of free DMDOHEMA molecules in the organic phase is close to that of the **HighC**1 simulation, 0.12 mol L^{-1} (*vs.* 0.08 mol L^{-1} for **HighC**1).

To further assess the robustness of our results, we performed additional 100 ns production simulations starting from the final configurations of the NVT simulations discussed in this work. As already done,

the last 50 ns of these trajectories were analyzed to compute the average number of oligomers and the corresponding composition maps. At a given concentration, fluctuations in the average number of oligomers were found to be more significant when using different initial configurations than when simply extending the simulation time (Fig. S13, SI). Nonetheless, the overall oligomer distributions remained similar across independent runs, except in the case of monomers for **HighC** simulations. This discrepancy arises from the presence of trimers and tetramers observed in the **HighC**2 system but not in **HighC**1. Similarly, aggregate stoichiometries showed greater variability across different starting points than with longer simulations, as illustrated in Figs. S14 and S15 (SI) and Table S1 (SI). However, as already pointed out, the stoichiometries at local equilibrium remained consistent. These findings support the conclusion that local equilibrium was reached in all cases. Full thermodynamic equilibrium, in contrast, likely requires simulation times beyond the reach of conventional molecular dynamics. It is worth noting that, for each concentration, a total of 400 ns of simulation time was accumulated across independent trajectories, highlighting the efficiency of this ensemble-based approach in sampling the relevant regions of phase space.

Our findings suggest that the starting point of the simulation, associated with a change in the initial micelle composition, influences only the size distribution of the aggregates and the number of large aggregates formed, not the local equilibrium average aggregate stoichiometries.

4. Conclusion

In the present paper, we investigated the formation of solvent extraction aggregates composed of $Eu(NO_3)_3$ salts with DMDOHEMA molecules solvated in *n*-heptane using classical molecular dynamics simulations. To understand the influence of the salt concentration on the aggregation properties, two organic phase compositions, based on experimental data obtained for two salt concentrations, were simulated, at 0.015 and 0.126 mol L^{-1} keeping the concentration of DMDOHEMA constant (0.5 mol L^{-1}). A detailed analysis of the compositions of aggregates highlighted that, for both $Eu(NO_3)_3$ concentrations, the main aggregates are predominantly in the form of Eu^{3+} monomers and dimers, with a higher ratio of monomers. However, increasing the $Eu(NO_3)_3$ concentration tends to increase the number of dimers. For both concentrations, the average Eu^{3+} monomer is composed of three nitrate anions and 3–4 DMDOHEMA molecules, the influence of the concentration being observable mainly on the number of water molecules involved in the monomers. Experimentally, the concentration of co-extracted water varies as a function of the $Eu(NO_3)_3$ concentration: it increases with the concentration of $Eu(NO_3)_3$. This is reflected in the composition of the monomers as we calculated average numbers of 4–5 and 2 water molecules in the Eu^{3+} monomers at 0.015 and 0.126 mol L^{-1}, respectively, which is close to or at the limiting Eu^{3+}:H_2O ratio of 1:5 for the **LowC** systems, and 1:2 for the **HighC** systems. The same trends have also been observed for the Eu^{3+} dimers. Indeed, at both $Eu(NO_3)_3$ concentrations, the dimer is composed on average of six nitrate anions, and six DMDOHEMA molecules. As already mentioned for the monomer, the influence of the $Eu(NO_3)_3$ concentration is only observed on the number of water molecules involved in the dimers: almost 18 and 4 at 0.015 and 0.126 mol L^{-1}, respectively. We demonstrated that the presence of the nitrate anions and water molecules in the polar core of the aggregates promotes the formation of the dimers, as various types of connections between Eu^{3+} cations are observed, primarily consisting of nitrate and nitrate-water bridges. The $Eu(NO_3)_3$ concentration, which is related to the concentration of co-extracted water, is observed to significantly influence these connections. Indeed, at low concentration, where the number of water molecules per Eu^{3+} cation is higher than at high concentration, we observed that nearly all the bridges formed are nitrate-water bridges. However, the reduced number of dimers formed under these conditions indicates that the concentration of $Eu(NO_3)_3$ acts as a limiting factor in the aggregate formation mechanism.

These results were made possible by implicitly accounting for polarization in the Eu^{3+} cation environment via the use of an additional $1/r^4$ term in the non-bonded interactions, and by performing MD simulations long enough to ensure that we reached equilibrium, allowing us to provide reliable structures. This was confirmed by examining the influence of the starting point on the structures of the formed aggregates. Indeed, even when using different initial configurations with varying numbers of nitrate anions, water molecules and DMDOHEMA ligands in the Eu^{3+} first coordination, the same average stoichiometries of Eu^{3+} monomers and dimers are observed as a function of the $Eu(NO_3)_3$ concentration. The same observations concerning the presence of water molecules hold true: the dynamics of water in the vicinity of the cations, as well as the availability of ligands to form hydrogen bonds, play a crucial role in determining the nature and the number of the aggregates formed. This is actually evidenced by the fact that new structures are observed at high concentrations consisting of Eu^{3+} trimer and tetramer, although in much smaller proportions compared to the monomers and dimers.

These results provide insights into the formation mechanism of aggregates in solvent extraction, emphasizing both the dynamic nature of their formation and the long-range interaction effects. These effects are observed through the availability of counter-anions, water, and extractant molecules to form hydrogen bonds in the solvent extraction organic phase, these hydrogen bonds driving the connectivity patterns between the Eu^{3+} cations. This study highlights the importance of the co-extracted water in the structural and dynamical properties of solvent extraction aggregates, which can play a crucial role in the stability of these phases.

CRediT authorship contribution statement

Lara Žiberna: Writing – review & editing, Writing – original draft. **Philippe Guilbaud:** Writing – review & editing, Supervision, Project administration. **Erwann Guillam:** Writing – review & editing. **Magali Duvail:** Writing – review & editing, Supervision, Project administration.

Declaration of competing interest

The authors declare that they have no known competing financial interests or personal relationships that could have appeared to influence the work reported in this paper.

Acknowledgement

The authors thank CEA/DES and ISEC for financial support. We acknowledge the CEA Marcoule computing center.

Appendix A. Supplementary material

Text explaining the code development for the study of aggregates; Schematic representation of the algorithm used for characterizing the oligomers formed during the simulation; Schematic representation of the DMDOHEMA extractant molecule; Eu^{3+} – $C_{DMDOHEMA}$, Eu^{3+} – $N_{NO_3^-}$, Eu^{3+} – $O_{DMDOHEMA}$, Eu^{3+} – $O_{NO_3^-}$, and Eu^{3+} – O_{H_2O} RDFs calculated for the **LowC**1, **HighC**1, **LowC**2, and **HighC**2 simulations; H_{H_2O} – $O_{DMDOHEMA}$, H_{H_2O} – $N_{NO_3^-}$, and H_{H_2O} – O_{H_2O} RDFs calculated for the **LowC**1, **HighC**1, **LowC**2, and **HighC**2 simulations; Time-averaged distribution of H_2O and DMDOHEMA molecules in the Eu^{3+} first coordination shell calculated for the **LowC**1, **HighC**1, **LowC**2, and **HighC**2 systems; Average numbers of Eu^{3+} monomers, dimers, trimers and tetramers calculated for the **LowC**1, **HighC**1, **LowC**2, and **HighC**2 systems, from both the initial simulations and the additional 100 ns production runs; Composition maps of Eu^{3+} aggregates calculated from 100 ns additional simulations for the **LowC**1, **HighC**1, **LowC**2, and **HighC**2 systems; Average stoichiometries of the Eu^{3+} monomers and dimers, and number of water molecules in the Eu^{3+} first coordination shell calculated for the **LowC**1, **HighC**1, **LowC**2 and **HighC**2 systems, from both the initial simulations and the additional 100 ns production runs.

Supplementary data to this article can be found online at doi:10.1016/j.molliq.2025.128711.

Data availability

Data will be made available on request.

References

[1] C. Poinssot, C. Rostaing, S. Greandjean, B. Boullis, Recycling the actinides, the cornerstone of any sustainable nuclear fuel cycles, Procedia Chem. 7 (2012) 349–357, https://doi.org/10.1016/j.proche.2012.10.055

[2] R. Taylor, W. Bodel, L. Stamford, G. Butler, A review of environmental and economic implications of closing the nuclear fuel cycle-part one: wastes and environmental impacts, Energies 15 (4) (2022) https://doi.org/10.3390/en15041433

[3] R. Taylor, G. Mathers, A. Banford, The development of future options for aqueous recycling of spent nuclear fuels, Prog, Nucl. Energy 164 (2023) 104837, https://doi.org/10.1016/j.pnucene.2023.104837

[4] L.B. Silverio, W. de Queiroz Lamas, An analysis of development and research on spent nuclear fuel reprocessing, Energy Policy 39 (1) (2011) 281–289, https://doi.org/10.1016/j.enpol.2010.09.040

[5] M. Salvatores, G. Palmiotti, Radioactive waste partitioning and transmutation within advanced fuel cycles: achievements and challenges, prog, Part. Nucl. Phys. 66 (1) (2011) 144–166, https://doi.org/10.1016/j.ppnp.2010.10.001

[6] P. Baron, S. Cornet, E. Collins, G. DeAngelis, G.D. Cul, Y. Fedorov, J. Glatz, V. Ignatiev, T. Inoue, A. Khaperskaya, I. Kim, M. Kormilitsyn, T. Koyama, J. Law, H. Lee, K. Minato, Y. Morita, J. Uhlíř, D. Warin, R. Taylor, A review of separation processes proposed for advanced fuel cycles based on technology readiness level assessments, Prog, Nucl. Energy 117 (2019) 103091, https://doi.org/10.1016/j.pnucene.2019.103091

[7] W.B. Lanham, T.C. Runion, Purex Process for Plutonium and Uranium Recovery, Tech. rep., Oak Ridge National Lab (ORNL), Oak, Ridge, TN (United States) (1949, https://doi.org/10.2172/4165457

[8] B. Abécassis, F. Testard, T. Zemb, L. Berthon, C. Madic, Effect of n-octanol on the structure at the supramolecular scale of concentrated dimethyldioctylhexylethoxymalonamide extractant solutions, Langmuir 19 (17) (2003) 6638–6644, https://doi.org/10.1021/la034088g

[9] A.B. Patil, P.N. Pathak, V.S. Shinde, P.K. Mohapatra, Synthesis and evaluation of N,N'-dimethyl-N,N'-dicyclohexyl-malonamide (DMDCMA) as an extractant for actinides, Sep, Sci. Technol. 49 (18) (2014) 2927–2932, https://doi.org/10.1080/01496395.2014.943772

[10] E.A. Mowafy, H.F. Aly, Extraction behaviours of Nd(III), Eu(III), La(III), Am(III) and U(VI) with some substituted malonamides from nitrate medium, solvent extr, Ion Exch. 20 (2) (2002) 177–194, https://doi.org/10.1081/SEI-120003020

[11] B. Gannaz, R. Chiarizia, M.R. Antonio, C. Hill, G. Cote, Extraction of lanthanides(III) and Am(III) by mixtures of malonamide and dialkylphosphoric acid, solvent extr, Ion Exch. 25 (3) (2007) 313–337, https://doi.org/10.1080/07366290701285512

[12] D. Serrano-Purroy, P. Baron, B. Christiansen, J.-P. Glatz, C. Madic, R. Malmbeck, G. Modolo, First demonstration of a centrifugal solvent extraction process for minor actinides from a concentrated spent fuel solution, Sep, Purif. Technol. 45 (2005) 157–162, https://doi.org/10.1016/j.seppur.2005.03.001

[13] G. Modolo, H. Vijgen, D. Serrano-Purroy, B. Christiansen, R. Malmbeck, C. Sorel, P. Baron, DIAMEX counter-current extraction process for recovery of trivalent actinides from simulated high active concentrate, Sep, Sci. Technol. 42 (3) (2007) 439–452, https://doi.org/10.1080/01496390601120763

[14] S. Riaño, S.S. Foltova, K. Binnemans, Separation of neodymium and dysprosium by solvent extraction using ionic liquids combined with neutral extractants: batch and mixer-settler experiments, RSC Adv. 10 (2020) 307–316, https://doi.org/10.1039/C9RA08996A

[15] M. Vatin, M. Duvail, P. Guilbaud, J.-F. Dufrêche, Thermodynamics of malonamide aggregation deduced from molecular dynamics simulations, J. Phys. Chem. B 125 (13) (2021) 3409–3418, https://doi.org/10.1021/acs.jpcb.0c10865

[16] M.J. Servis, B. Sadhu, L. Soderholm, A.E. Clark, Amphiphile conformation impacts aggregate morphology and solution structure across multiple lengthscales, J. Mol. Liq. 345 (2022) 117743, https://doi.org/10.1016/j.molliq.2021.117743

[17] P. Weßling, M. Trumm, A. Geist, P.J. Panak, Stoichiometry of an(III)–DMDOHEMA complexes formed during solvent extraction, Dalton Trans. 47 (2018) 10906–10914, https://doi.org/10.1039/C8DT02504E

[18] F. Testard, P. Bauduin, L. Martinet, B. Abécassis, L. Berthon, C. Madic, T. Zemb, Self-assembling properties of malonamide extractants used in separation processes, Radiochim, Acta 96 (4–5) (2008) 265–272, https://doi.org/10.1524/ract.2008.1487

[19] R.J. Ellis, Y. Meridiano, J. Muller, L. Berthon, P. Guilbaud, N. Zorz, M.R. Antonio, T. Demars, T. Zemb, Complexation-induced supramolecular assembly drives metal-ion extraction, Chem.–Eur. J. 20 (40) (2014) 12796–12807, https://doi.org/10.1002/chem.201403859

[20] C. Micheau, Y. Ueda, R. Motokawa, K. Akutsu-Suyama, N.L. Yamada, M. Yamada, S.A. Moussaoui, E. Makombe, D. Meyer, L. Berthon, D. Bourgeois, Organization of malonamides from the interface to the organic bulk phase, J. Mol. Liq. 401 (2024) 124372, https://doi.org/10.1016/j.molliq.2024.124372

[21] C. Bauer, P. Bauduin, J.-F. Dufrêche, T. Zemb, O. Diat, Liquid/liquid metal extraction: phase diagram topology resulting from molecular interactions between extractant, ion, oil and water, Eur. Phys. J. Spec. Top. 213 (2012) 225–241, https://doi.org/10.1140/epjst/e2012-01673-4

[22] Y. Meridiano, L. Berthon, X. Crozes, C. Sorel, P. Dannus, M.R. Antonio, R. Chiarizia, T. Zemb, Aggregation in organic solutions of malonamides: consequences for water extraction, solvent extr, Ion Exch. 27(5-6) (2009) 607–637, https://doi.org/10.1080/07366290903270148

[23] M. Bley, B. Siboulet, A. Karmakar, T. Zemb, J.-F. Dufrêche, A predictive model of reverse micelles solubilizing water for solvent extraction, J. Colloid Interface Sci. 479 (2016) 106–114, https://doi.org/10.1016/j.jcis.2016.06.044

[24] L. Berthon, F. Testard, L. Martinet, T. Zemb, C. Madic, Influence of the extracted solute on the aggregation of malonamide extractant in organic phases: consequences for phase stability, C. R. Chim. 13 (10) (2010) 1326–1334, https://doi.org/10.1016/j.crci.2010.03.024

[25] R.J. Ellis, M.R. Antonio, Coordination structures and supramolecular architectures in a cerium(III)-malonamide solvent extraction system, Langmuir 28 (2012) 5987–5998, https://doi.org/10.1021/la3002916

[26] P. Guilbaud, T. Zemb, Solute-induced microstructural transition from weak aggregates towards a curved film of surface-active extractants, ChemPhyschem. 13 (3) (2012) 687–691, https://doi.org/10.1002/cphc.201100721

[27] M.J. Servis, M. Piechowicz, L. Soderholm, Impact of water extraction on malonamide aggregation: a molecular dynamics and graph theoretic approach, J. Phys. Chem. B 125 (24) (2021) 6629–6638, https://doi.org/10.1021/acs.jpcb.1c02962

[28] B. Qiao, K.C. Littrell, R.J. Ellis, Liquid worm-like and proto-micelles: water solubilization in amphiphile–oil solutions, Phys. Chem. Chem. Phys. 20 (2018) 12908–12915, https://doi.org/10.1039/C8CP00600H

[29] R.J. Ellis, Y. Meridiano, R. Chiarizia, L. Berthon, J. Muller, L. Couston, M.R. Antonio, Periodic behavior of lanthanide coordination within reverse micelles, Chem.–Eur. J. 19 (8) (2013) 2663–2675, https://doi.org/10.1002/chem.201202880

[30] B.L. Bonnett, D. Sheyfer, P.N. Wimalasiri, S. Nayak, J. Lal, Q. Zhang, S. Seifert, G.B. Stephenson, M.J. Servis, Critical fluctuations in liquid–liquid extraction organic phases controlled by extractant and diluent molecular structure, Phys. Chem. Chem. Phys. 25 (2023) 16389–16403, https://doi.org/10.1039/D3CP01029E

[31] S. Nave, C. Mandin, L. Martinet, L. Berthon, F. Testard, C. Madic, T. Zemb, Supramolecular organisation of tri-n-butyl phosphate in organic diluent on approaching third phase transition, Phys. Chem. Chem. Phys. 6 (4) (2004) 799–808, https://doi.org/10.1039/B311702B

[32] K. Osseo-Asare, Aggregation, reversed micelles, and microemulsions in liquid-liquid extraction: the tri-n-butyl phosphatediluent-water-electrolyte system, Adv. Colloid Interface Sci. 37 (1) (1991) 123–173, https://doi.org/10.1016/0001-8686(91)80041-H

[33] L. Berthon, L. Martinet, F. Testard, C. Madic, T. Zemb, Solvent penetration and sterical stabilization of reverse aggregates based on the DIAMEX process extracting molecules: consequences for the third phase formation, solvent extr, Ion Exch. 25 (5) (2007) 545–576, https://doi.org/10.1080/07366290701512576

[34] R. Poirot, D. Bourgeois, D. Meyer, Palladium extraction by a malonamide derivative (DMDOHEMA) from nitrate media: extraction behavior and third phase characterization, solvent extr, Ion Exch. 32 (5) (2014) 529–542, https://doi.org/10.1080/07366299.2014.908587

[35] M. Duvail, D.M. Martinez, L. Žiberna, E. Guillam, J.-F. Dufrêche, P. Guilbaud, Modeling lanthanide ions in solution: a versatile force field in aqueous and organic solvents, J. Chem. Theory. Comput. 20 (3) (2024) 1282–1292, https://doi.org/10.1021/acs.jctc.3c01162

[36] D.A. Case, K. Belfon, I.Y. Ben-Shalom, S.R. Brozell, D. Cerutti, I.T.E. Cheatham, V.W.D. Cruzeiro, T.A. Darden, R.E. Duke, G. Giambasu, M.K. Gilson, H. Gohlke, A.W. Goetz, R. Harris, S. Izadi, S.A. Izmailov, K. Kasavajhala, A. Kovalenko, R. Krasny, T. Kurtzman, T.S. Lee, S. LeGrand, P. Li, C. Lin, J. Liu, T. Luchko, R. Luo, V. Man, K.M. Merz, Y. Miao, O. Mikhailovskii, G. Monard, H. Nguyen, A. Onufriev, F. Pan, S. Pantano, R. Qi, D.R. Roe, A. Roitberg, C. Sagui, S. Schott-Verdugo, J. Shen, C.L. Simmerling, N.R. Skrynnikov, J. Smith, J. Swails, R.C. Walker, J. Wang, L. Wilson, R.M. Wolf, X. Wu, Y. Xiong, Y. Xue, D.M. York, P.A. Kollman, Amber 2020, university of California, San Francisco (2020).

[37] S. Izadi, R. Anandakrishnan, A.V. Onufriev, Building water models: a different approach, J. Phys. Chem. Lett. 5 (21) (2014) 3863–3871, https://doi.org/10.1021/jz501780a

[38] P. Li, K.M. Merz, Taking into account the ion-induced dipole interaction in the nonbonded model of ions, J. Chem. Theory Comput. 10 (1) (2014) 289–297, https://doi.org/10.1021/ct400751u

[39] P. Li, L.F. Song, K.M. Merz, Parameterization of highly charged metal ions using the 12-6-4 LJ-type nonbonded model in explicit water, J. Phys. Chem. B 119 (3) (2015) 883–895, https://doi.org/10.1021/jp505875v

[40] P. Li, L.F. Song, K.M. Merz, Systematic parameterization of monovalent ions employing the nonbonded model, J. Chem. Theory. Comp. 11 (4) (2015) 1645–1657, https://doi.org/10.1021/ct500918t

[41] Z. Li, L.F. Song, P. Li, K.M. Merz, Parametrization of trivalent and tetravalent metal ions for the OPC3, OPC, TIP3P-FB, and TIP4P-FB water models, J. Chem. Theory. Comp. 17 (2021) 2342–2354.

[42] D.M. Martinez, D. Guillaumont, P. Guilbaud, Force field parameterization of actinyl molecular cations using the 12-6-4 model, J. Chem. Inf. Model. 62 (10) (2022) 2432–2445, https://doi.org/10.1021/acs.jcim.2c00153

[43] P. Li, B.P. Roberts, D.K. Chakravorty, K.M. Merz, Rational design of particle mesh Ewald compatible Lennard-Jones parameters for +2 metal cations in explicit solvent, J. Chem. Theory Comput. 9 (2013) 2733–2748, https://doi.org/10.1021/CT400146W

[44] D.S. Eisenberg, W. Kauzmann, The Structure and Properties of Water, Oxford University Press, 1969.

[45] K.J. Miller, Additivity methods in molecular polarizability, J. Am. Chem. Soc. 112 (23) (1990) 8533–8542, https://doi.org/10.1021/ja00179a044

[46] H.J.C. Berendsen, J.P.M. Postma, W.F. van Gunsteren, A. DiNola, J.R. Haak, Molecular dynamics with coupling to an external bath, J. Chem. Phys. 81 (8) (1984) 3684–3690, https://doi.org/10.1063/1.448118
[47] T. Darden, D. York, L. Pedersen, Particle mesh Ewald: an $N \cdot \log(N)$ method for Ewald sums in large systems, J. Chem. Phys. 98 (12) (1993) 10089–10092, https://doi.org/10.1063/1.464397
[48] L. Martínez, R. Andrade, E.G. Birgin, J.M. Martínez, PACKMOL: a package for building initial configurations for molecular dynamics simulations, J. Comput. Chem. 30 (13) (2009) 2157–2164, https://doi.org/10.1002/jcc.21224
[49] W. Humphrey, A. Dalke, K. Schulten, VMD – Visual Molecular Dynamics, J. Mol. Graph. 14 (1996) 33–38, https://doi.org/10.1016/0263-7855(96)00018-5
[50] N. Michaud-Agrawal, E.J. Denning, T.B. Woolf, O. Beckstein, Mdanalysis: a toolkit for the analysis of molecular dynamics simulations, J. Comput. Chem. 32 (10) (2011) 2319–2327, https://doi.org/10.1002/jcc.21787
[51] R.J. Gowers, M. Linke, J. Barnoud, T.J.E. Reddy, M.N. Melo, S.L. Seyler, J. Domański, D.L. Dotson, S. Buchoux, I.M. Kenney, O. Beckstein, Mdanalysis: a Python package for the rapid analysis of molecular dynamics simulations, in: S. Benthall, S. Rostrup (Eds.), Proceedings of the 15th Python in Science Conference, 2016, pp. 98–105, https://doi.org/10.25080/Majora-629e541a-00e
[52] B. Qiao, T. Demars, M. Olvera de la Cruz, R.J. Ellis, How hydrogen bonds affect the growth of reverse micelles around coordinating metal ions, J. Phys. Chem. Lett. 5 (8) (2014) 1440–1444, https://doi.org/10.1021/jz500495p
[53] B. Qiao, G. Ferru, M. Olvera de la Cruz, R.J. Ellis, Molecular origins of mesoscale ordering in a metalloamphiphile phase, ACS Cent. Sci. 1 (9) (2015) 493–503, https://doi.org/10.1021/acscentsci.5b00306
[54] J.M. Muller, C. Berthon, L. Couston, D. Guillaumont, R.J. Ellis, N. Zorz, J.-P. Simonin, L. Berthon, Understanding the synergistic effect on lanthanides(III) solvent extraction by systems combining a malonamide and a dialkyl phosphoric acid, Hydrometallurgy 169 (2017) 542–551, https://doi.org/10.1016/j.hydromet.2017.02.012
[55] Y. Meridiano, L. Berthon, S. Lagrave, X. Crozes, C. Sorel, F. Testard, T. Zemb, Correlation between aggregation and extracting properties in solvent extraction systems: extraction of actinides(III) and lanthanides(III) by a malonamide in non acidic media, in: I. A. E. A (IAEA) (Ed.), Nuclear Fuel Cycle for a Sustainable Future (Atalante 2008), Montpellier, France, 2008, pp. O3 1–8. https://inis.iaea.org/records/y1q75-env10 .
[56] M. Duvail, P. Guilbaud, Understanding the nitrate coordination to Eu^{3+} ions in solution by potential of mean force calculations, Phys. Chem. Chem. Phys. 13 (2011) 5840–5847, https://doi.org/10.1039/C0CP02535F